Electronic Supporting Information

Heavy-atom Doping Thermally Activated Delayed Fluorophores Cesium Zirconium Halides for Efficient X-Ray Imaging

Dandan Yang,*[a] Ling Li,[a] Shijia Liu,[a] Xudong Hu,[b] Xuebin Zhang,[a] Zhiheng Xu,*[c] Shiying Guo,[d] Bing Wang,[e] Xiaobin Tang,[c] Zhuang Chen,[d] Xiaoming Li,*[b] Qin Xu,*[a] Haibo Zeng[a,b]

[a] *Institute of Innovation Materials and Energy, School of Chemistry and Chemical Engineering, Yangzhou University, Yangzhou, 225002, China.*

[b] *MIIT Key Laboratory of Advanced Display Materials and Devices, Institute of Optoelectronics & Nanomaterials, College of Materials Science and Engineering, Nanjing University of Science and Technology, Nanjing, 210094, China.*

[c] *Department of Nuclear Science and Technology, Key Laboratory of Nuclear Technology Application and Radiation Protection in Astronautics, Ministry of Industry and Information Technology, Nanjing University of Aeronautics and Astronautics, Nanjing, 211106, China.*

[d] *College of Physics Science and Technology, Yangzhou University, Yangzhou, 225002, China.*

[e] *Hubei University of Automotive Technology, Shiyan, 442002, China.*

Experimental Section

Materials: Cesium chloride (CsCl, 99.99%), Hafnium chloride ($HfCl_4$, 99.9%), Zirconium chloride ($ZrCl_4$, 99.9%), and PDMS were purchased from Aladdin Industrial Corporation. Isopropanol and hydrochloric acid (HCl, 37%) were purchased from Sinopharm Chemical Reagent Company. All chemicals were used as received without further purification.

Preparation of $Cs_2Zr_{1-x}Cl_6$: xHf: 2 mmol CsCl was first dissolved in 5 mL HCl solution in 25 mL Teflon autoclave. Then x mmol of $HfCl_4$ and 1-x mmol $ZrCl_4$ were added and the solution was heated at 100°C for 12 h. The solution was then gradually cooled to room temperature. The as-synthesized samples were then filtered out, washed by isopropanol, and dried in a vacuum drying oven at 60°C for overnight.

Preparation of $Cs_2Zr_{1-x}Cl_6$:xHf scintillators: The PDMS was prepared by mixing the pre-polymer and curing agent at a volume ratio of 10: 1. Then, the Cs_2ZrCl_6 powder and PDMS were mixed uniformly at a mass ratio of 1:2. The mixture was dropped onto a glass storage base and spin-coated into dense and uniform films. Following that, the prepared films were cured in an oven at 60 °C for a period, obtaining a uniform film. The different thickness of films can be controlled by controlling the number of spin-coatings.

Characterizations: The X-ray diffraction (XRD) was performed on a D8 ADVANCE diffractometer. The scanning electron microscopy (SEM, Zeiss Sigma 55) was used to observe the morphology. The elemental composition and chemical state were identified by X-ray photoelectron spectroscopy (XPS ESCALAB 250X). The UV-VIS-NIR spectrophotometer (Cary 5000) was used to measure the absorption spectra. The PL and PLE spectra, temperature-dependent PL spectra were measured with the Horiba Jobin Yvon Fluorolog-3 spectrometer. The PLQY was determined using a Quantaurus-QY absolute photoluminescence quantum yield spectrometer (C11347-11, Hamamatsu Photonics, Japan). The time-resolved decay data were performed on an Edinburgh FLS1000 fluorescence spectrometer.

Fitting of temperature-dependent PL

Thermal activation process: The emission intensity increases as the temperature increases (77 K-237 K). The increase of emission may be caused by thermal activation of electrons in triplet state overcoming Ea_1 to singlet state. Thus, the lower thermal activation energy, the easier it goes over the energy barrier, and the more likely to promote the energy transfer from triplet state to singlet state. The integrated emission intensity(I) versus inverse temperature ($1/T$) can be expressed as:

$$I(T) = I_0 \Big/ \left[1 + Ae^{\left(E_{a1}/Tk_B\right)}\right] \quad (1)$$

where I_0 represents the intensity at 0 K, k_B denotes the Boltzmann constant, and E_{a1} is the energy gap.

Thermal quenching process: The emission spectra show a subsequent thermal quenching with a further increase in the temperature (237 K-377 K). With a further increase in the temperature (≥237 K), other nonradiative decay processes start to play an important role. The higher thermal activation energy Ea_2 indicates that the exciton dissociation process requires more energy, and nonradiative recombination

can be suppressed, which is beneficial for radiative recombination. The integrated emission intensity(*I*) versus inverse temperature (1/*T*) can be expressed as:

$$I(T) = I_0 \Big/ \left[1 + Ae^{(-E_{a2}/Tk_B)}\right] \quad (2)$$

where I_0 represents the intensity at 0 K, k_B denotes the Boltzmann constant, and E_{a2} is the activation energy.

Light yield measurement: The samples are placed successively in an integrating sphere at a certain distance from the X-ray source to unify the radiation dose and field. The scintillation spectrum is directly collected by the fiber coupled fluorescence spectrometer.

$$\frac{LY_1}{LY_{CsI:Tl}} = \frac{R_{CsI:Tl}}{R_1} \times \frac{\int I_1(\lambda)S(\lambda)d\lambda \times S_1 \times D_1}{\int I_{CsI:Tl}(\lambda)S(\lambda)d\lambda \times S_{CsI:Tl} \times D_{CsI:Tl}}$$

Where *R* is the percentage of X-ray deposition energy of the scintillator, *S* represents the wavelength dependent detection efficiency of SiPM, and $I(\lambda)$ represent the RL spectrum of scintillators measured by a fiber optic spectrometer. *S* is the irradiated area and *D* is the sample thickness. Since the X-rays from the sample are thick enough to be fully absorbed, the sample box makes the irradiated sample area have the same geometric shape and size to eliminate errors. It is known that the light yield of CsI:Tl single crystal is 54000 Photons per MeV, and the light yield is estimated directly according to the above formula. The calculated light yield was 57000 Photons per MeV.

Modulation Transfer function (MTF) calculation: MTF determines the spatial resolution of imaging system and represents the ability to transfer input signal modulation of spatial frequency relative to its output. The MTF value of 1 indicates the perfect detection of a given spatial frequency. Using slanted-edge method to calculate MTF, we took the X-ray images of a sharp edge from a piece of tungsten (thickness: ~1mm), and the X-ray dose rate was 2 $mGy_{air}\ s^{-1}$. Next the edge spread function (ESF) was derived by the edge profile, from which we could deduce the line spread function (LSF) by calculating derivative. Finally, the Fourier transform of the LSF defines the MTF, meaning the MTF curves could be calculated by the following formula:

$$MTF(v) = F(LSF(x)) = F\left(\frac{dESF(x)}{dx}\right)$$

Where *v* is spatial frequency, *x* is the position of pixels.

Figure S1. Schematic diagram of the synthesis process of Cs_2ZrCl_6:xHf powders by solvothermal method.

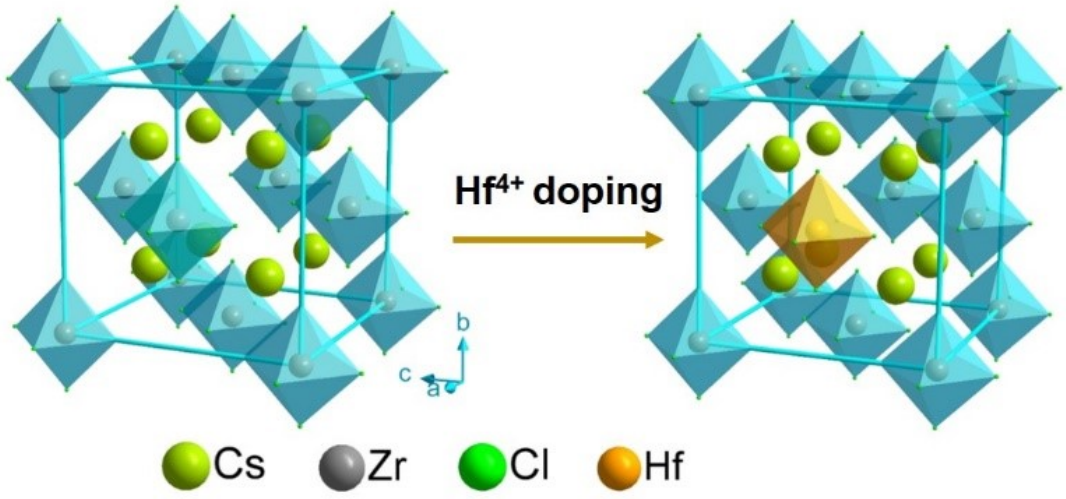

Figure S2. Crystal structure diagram of pure and Hf doping Cs_2ZrCl_6.

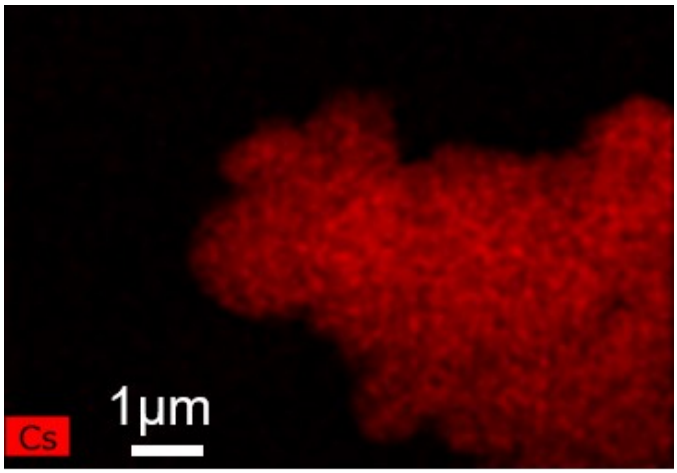

Figure S3. Cs element mapping image of Cs_2ZrCl_6:0.8%Hf sample.

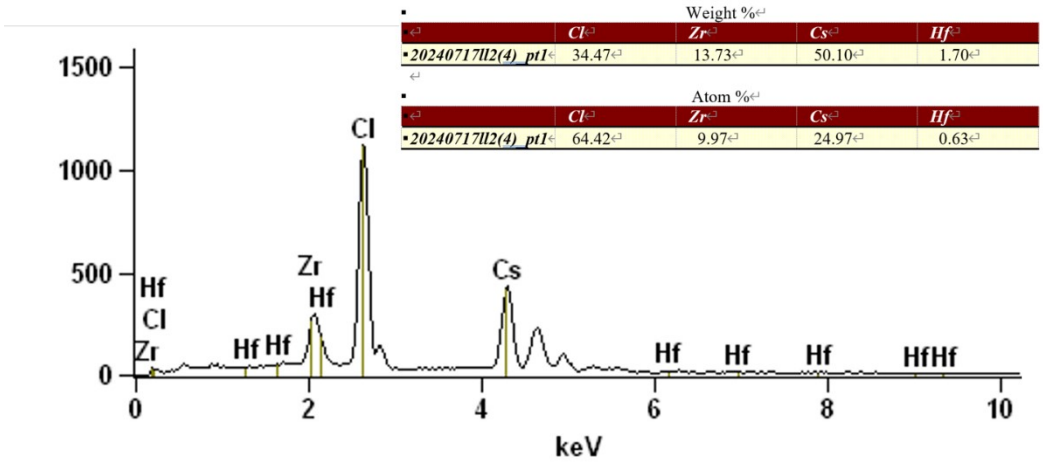

Figure S4. The EDS spectrum of Cs_2ZrCl_6:0.8%Hf sample.

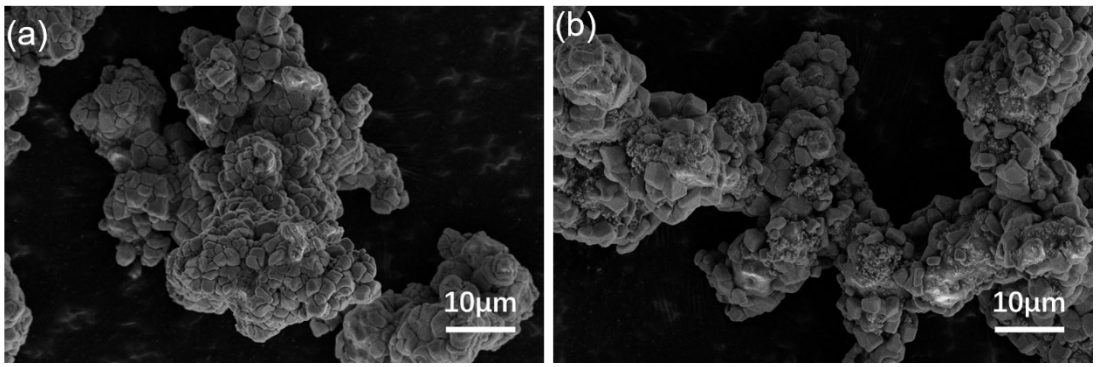

Figure S5. The SEM images of (a) Cs_2ZrCl_6 and (b) Cs_2ZrCl_6:0.8%Hf.

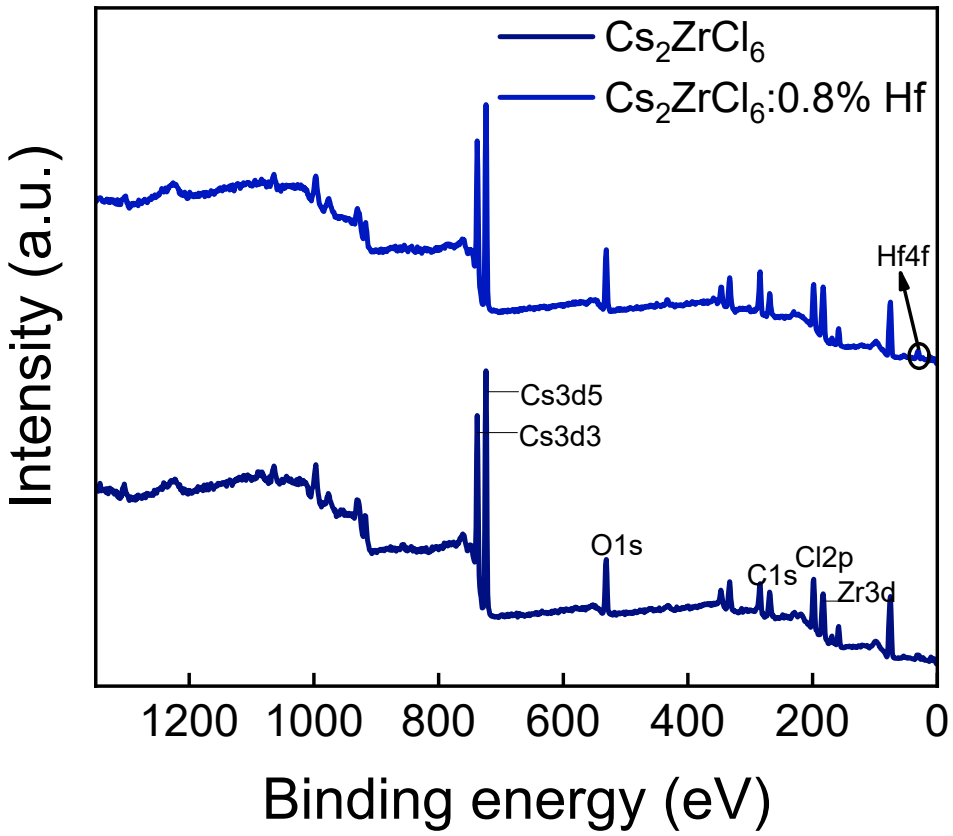

Figure S6. The XPS survey spectra of Cs_2ZrCl_6 and Cs_2ZrCl_6:0.8%Hf.

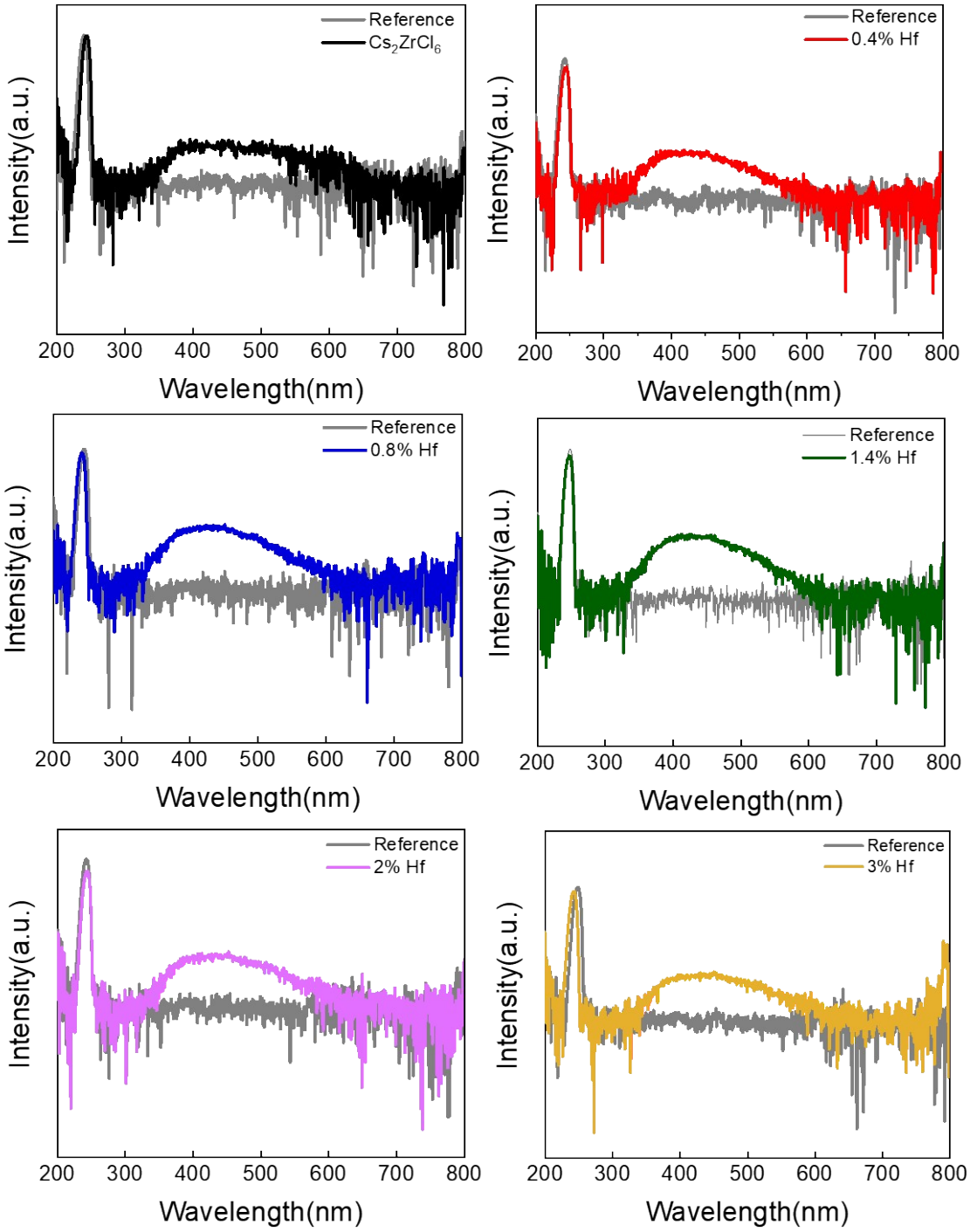

Figure S7. The PLQY values of Cs_2ZrCl_6:xHf (x=0-3%).

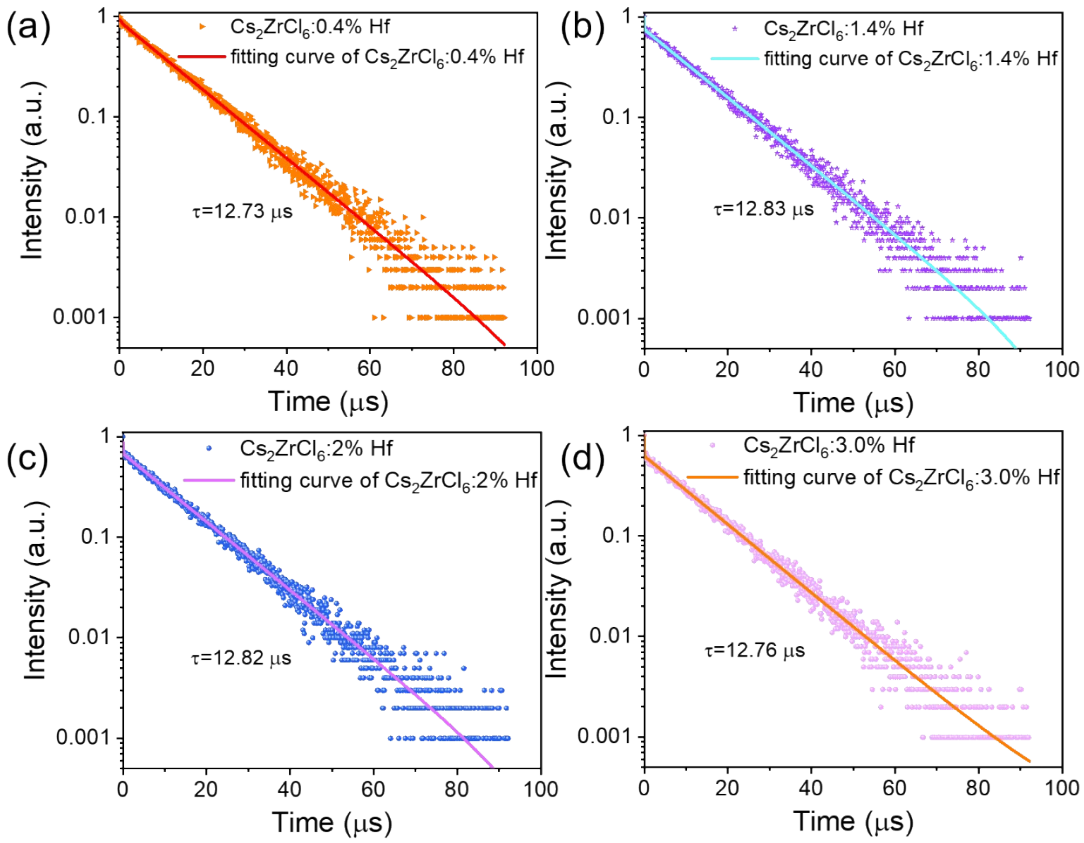

Figure S8. PL decay curves of Cs_2ZrCl_6:xHf (x=0.4%, 1.4%, 2.0%, and 3.0%) samples under 254 nm excitation and monitoring wavelength of 438 nm.

Table S1. PL decay lifetime of Cs_2ZrCl_6:xHf (x=0-3%).

Samples	A_1	$\tau_1(\mu s)$	A_2	$\tau_2(\mu s)$	$\tau(\mu s)$	R^2
0%	0.3361	0.000497	0.605	12.68	12.68	0.995
0.4%	0.04355	0.748	0.891	12.77	12.73	0.996
0.8%	-	-	0.930	12.87	12.87	0.997
1.4%	0.2520	0.0219	0.748	12.83	12.83	0.996
2.0%	0.2025	0.0029	0.675	12.82	12.82	0.995
3.0%	0.3648	0.00268	0.621	12.76	12.76	0.996

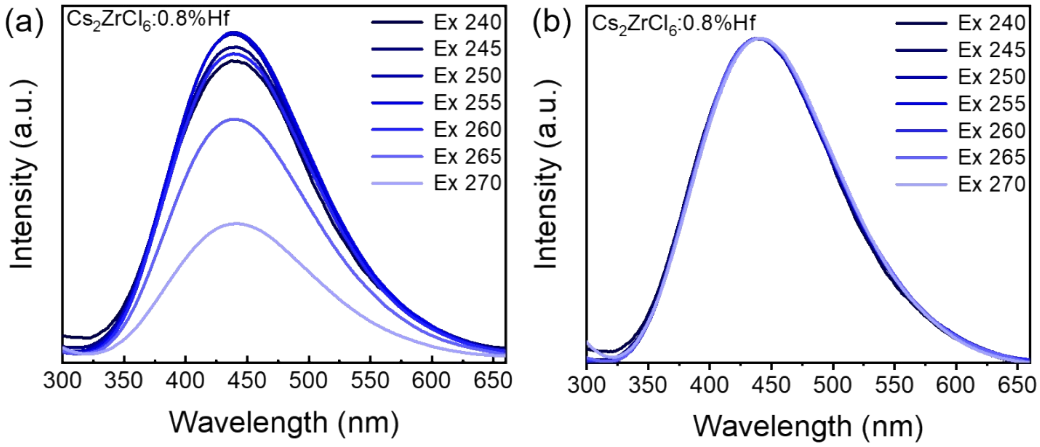

Figure S9. The (a) original and (b) normalized PL spectra of Cs_2ZrCl_6:0.8% Hf sample under different excitation wavelength.

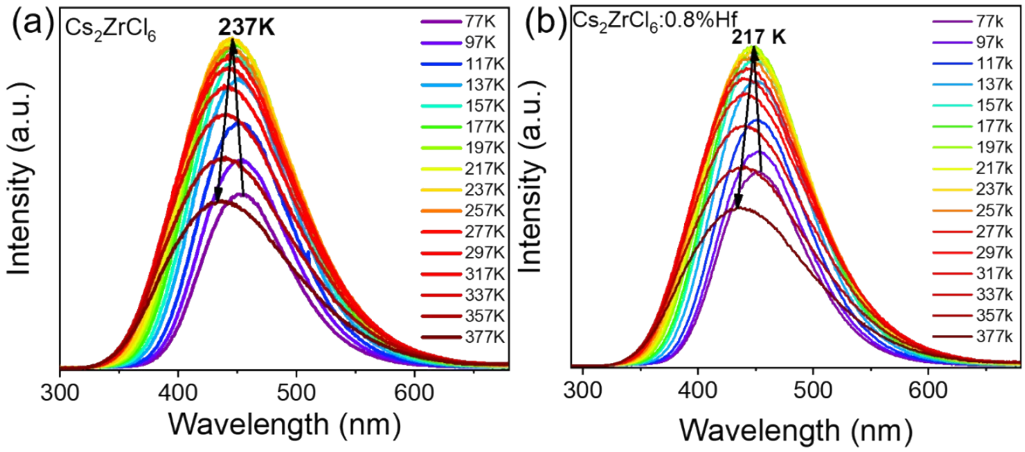

Figure S10. The temperature-dependent PL spectra of (a) Cs_2ZrCl_6 and (b) Cs_2ZrCl_6:0.8%Hf measured from 77 K to 377 K.

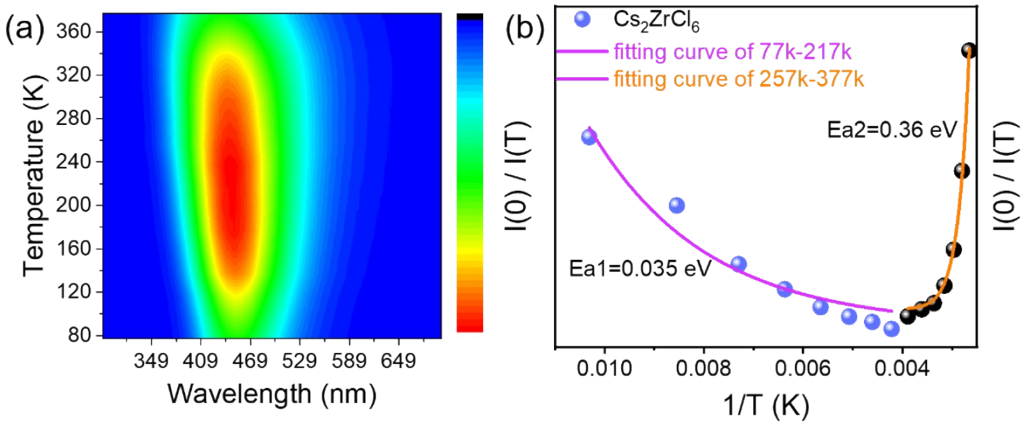

Figure S11. (a) The pseudo color map of the PL spectra of Cs_2ZrCl_6 sample under 260 nm excitation. (b) The relationships between *I(0)/I(T)* versus *1/T* (T=77 K-377 K) and the two linear fitting results for

Cs_2ZrCl_6 sample.

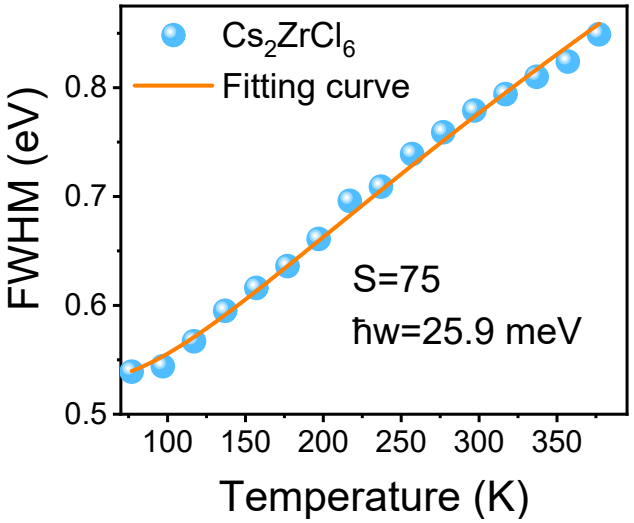

Figure S12. Fitting curve of the *FWHM* as a function of temperature (T=77 K-377 K) for Cs_2ZrCl_6 sample.

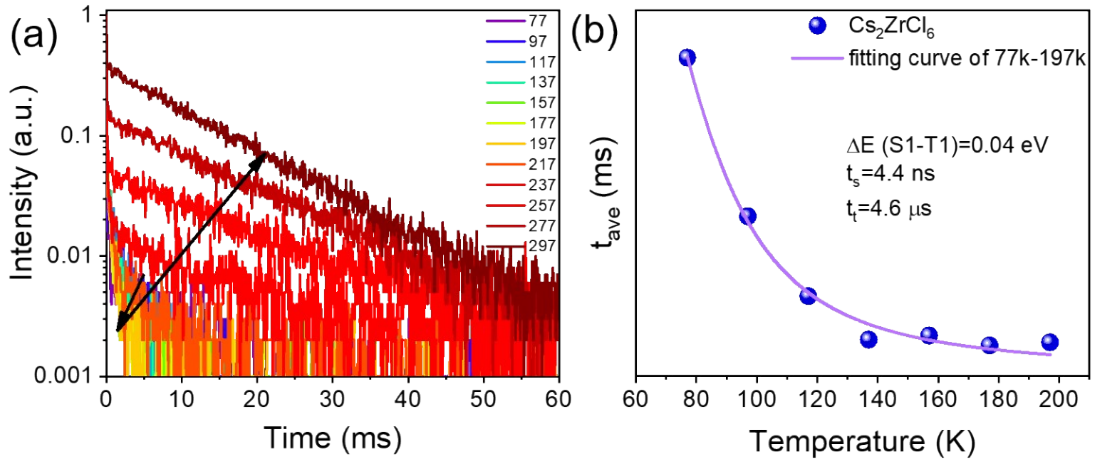

Figure S13. (a) Temperature-dependent PL decay curves of Cs_2ZrCl_6 measured from 77 K to 297 K. (b) Fitting curve of τ_{ave} as a function of T (T=77 K-217 K) for Cs_2ZrCl_6.

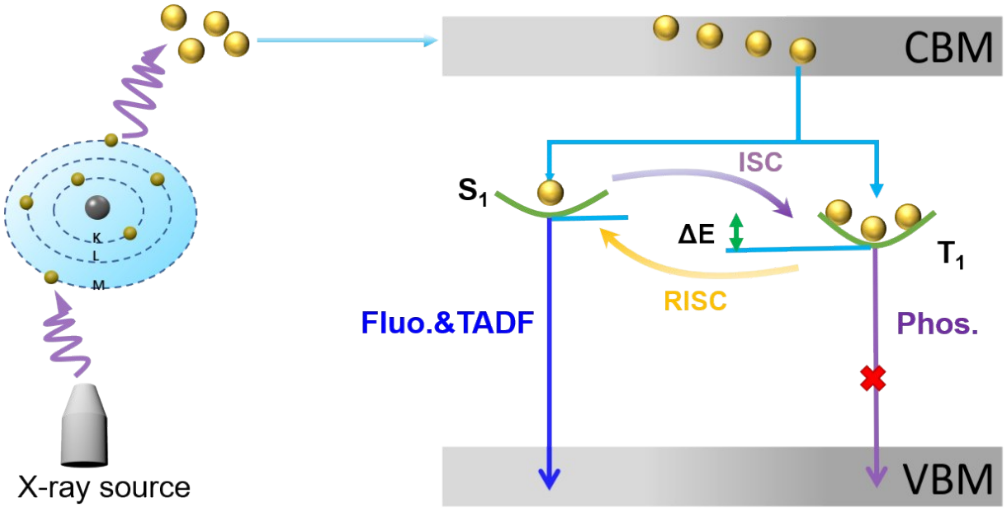

Figure S14. The schematic mechanism of the X-ray-induced scintillation process in Cs_2ZrCl_6:0.8%Hf scintillator.

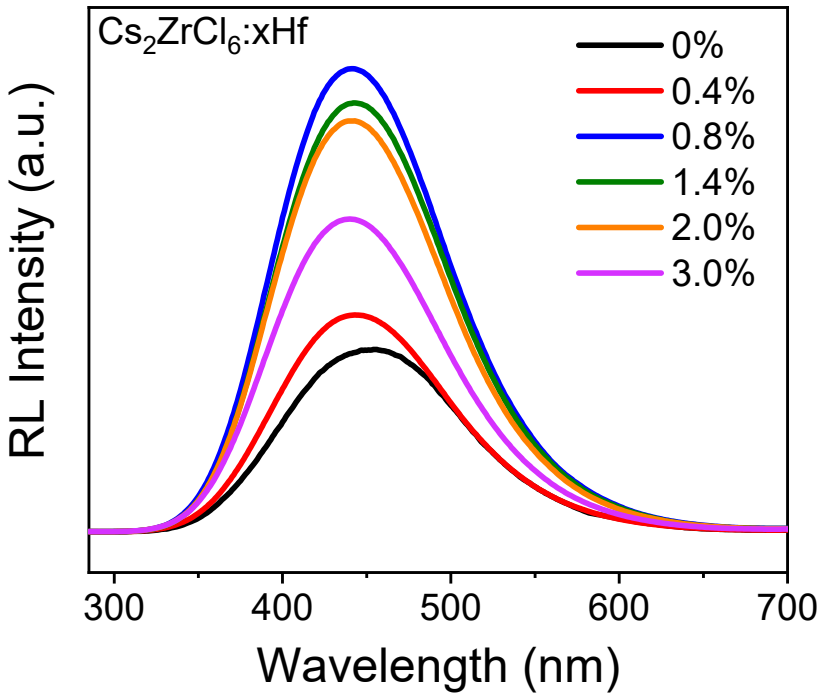

Figure S15. The RL intensity of Cs_2ZrCl_6:xHf (x=0-3%) samples.

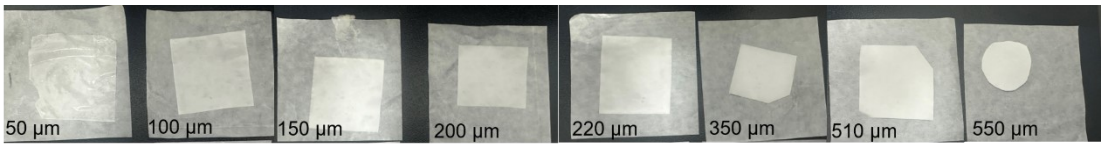

Figure S16. The physical photos of Cs_2ZrCl_6:0.8% Hf films with different thicknesses (50 μm -550 μm).

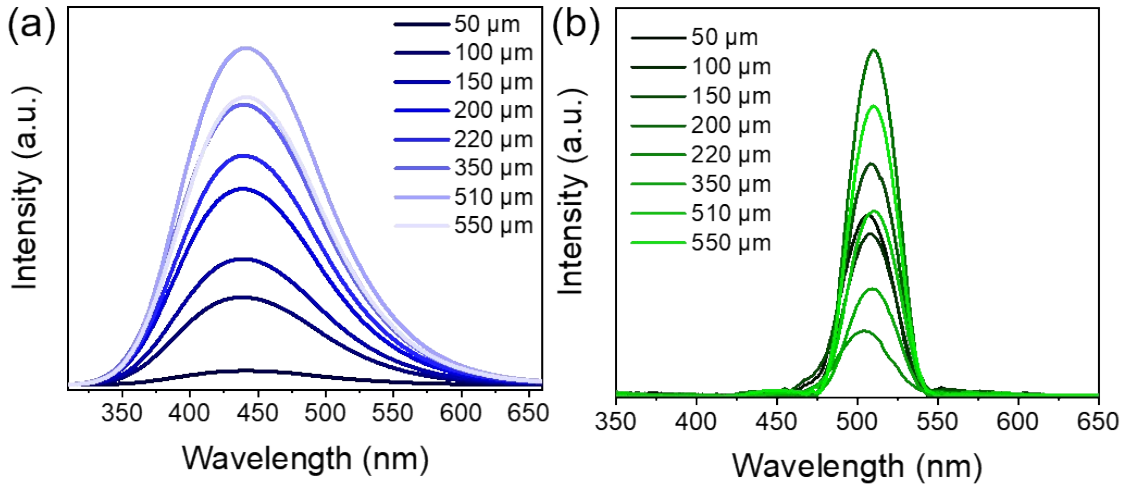

Figure S17. The RL intensity of (a) Cs_2ZrCl_6:0.8%Hf and (b) $CsPbBr_3$ NWs samples with different

thicknesses (50 µm -550 µm).

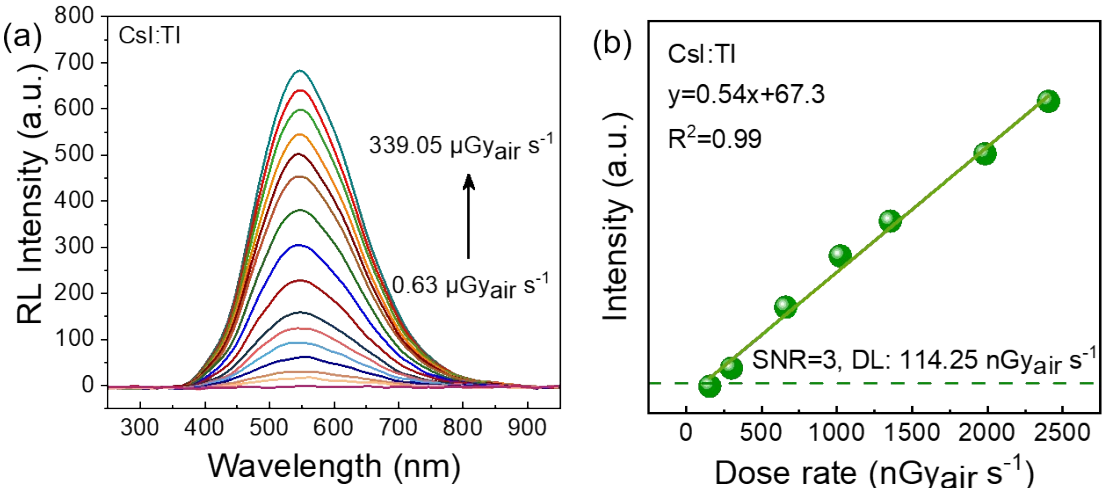

Figure S18. (a) RL spectra of CsI:Tl under X-ray radiation at different dose rates. (b) The plotted RL intensity of CsI:Tl as a function of X-ray dose rate.

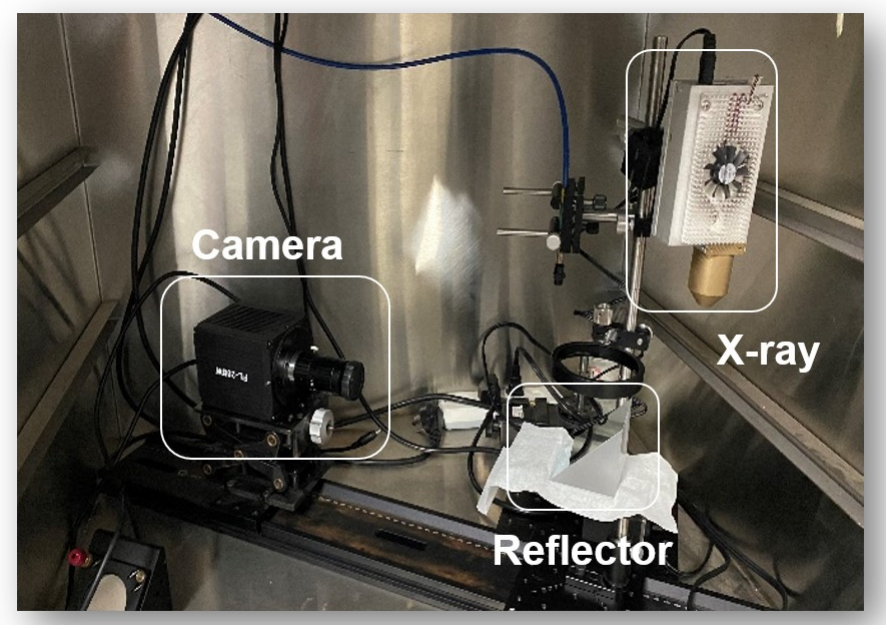

Figure S19. Devices constructed for prototype X-ray imaging.

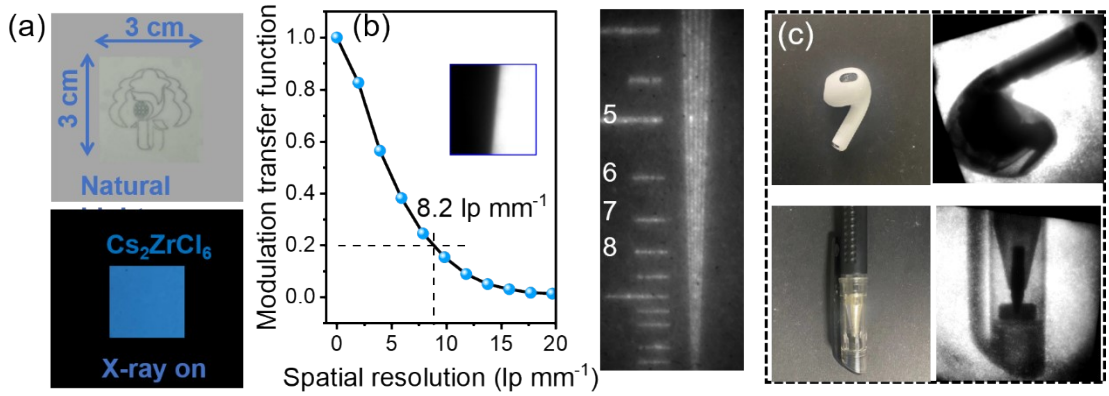

Figure S20. (a) Cs_2ZrCl_6 film under natural light and X-rays. (b) MTF calculation of Cs_2ZrCl_6 scintillator film and image of the line-pair card under X-ray radiation. (c) Photograph and X-ray imaging of Cs_2ZrCl_6 scintillator conducted by Bluetooth and ballpoint pen head.